Results in Physics 8 (2018) 357–364

Contents lists available at ScienceDirect

Results in Physics

journal homepage: www.journals.elsevier.com/results-in-physics

On framing potential features of SWCNTs and MWCNTs in mixed convective flow

T. Hayat [a,b], Siraj Ullah [a,*], M. Ijaz Khan [a], A. Alsaedi [b]

[a] Department of Mathematics, Quaid-I-Azam University 45320, 44000, Pakistan
[b] Nonlinear Analysis and Applied Mathematics (NAAM) Research Group, Department of Mathematics, Faculty of Science, King Abdulaziz University, P.O. Box 80257, Jeddah 21589, Saudi Arabia

ARTICLE INFO

Article history:
Received 17 November 2017
Received in revised form 5 December 2017
Accepted 7 December 2017
Available online 16 December 2017

Keywords:
Porous medium
SWCNTs and MWCNTs
Viscous dissipation
Melting heat transfer
Non-linear thermal radiation

ABSTRACT

Our target in this research article is to elaborate the characteristics of Darcy-Forchheimer relation in carbon–water nanoliquid flow induced by impermeable stretched cylinder. Energy expression is modeled through viscous dissipation and nonlinear thermal radiation. Application of appropriate transformations yields nonlinear ODEs through nonlinear PDEs. Shooting technique is adopted for the computations of nonlinear ODEs. Importance of influential variables for velocity and thermal fields is elaborated graphically. Moreover rate of heat transfer and drag force are calculated and demonstrated through Tables. Our analysis reports that velocity is higher for ratio of rate constant and buoyancy factor when compared with porosity and volume fraction.

Introduction

A carbon nanotube being shaped material which is isotope of carbon with a cylindrical nanostructure, having a diameter measuring on the nanometer scale. Carbon nanotubes can be subdivided into two categories depending on the structure namely (SWCNTs) and (MWCNTs). Carbon nanotubes have extensive applications in engineering, prostheses, genomics, pharmacogenomics, drug delivery, surgery and general medicine. Choi et al. [1] investigated thermal conductivity enhancement in nanotube suspension. They considered oil based nanoliquids comprising carbon nanotubes and found that nanotubes yields remarkable thermal conductivity enhancement. Impact of non-Fourier heat flux on unsteady chemically reactive flow of SMCNTs and MWCNTs is presented by Hayat et al. [2] They considered Xue model for the effectual thermal conductivity of nanoliquid. They also investigated that Nusselt number enhances for rising values of thermal relaxation and curvature parameters. MHD flow of carbon water nanomaterials with Marangoni convective and thermal radiation due to stretchable disk is examined by Mahanthesh et al. [3]. They implemented Runge–Kutta method through shooting approach to find out the numerical solutions of nonlinear expressions. Their results illustrated that the Nusselt number enhances for larger estimation of Marangoni number and nanoparticles volume fraction while it decays for Hartman number. MHD slip flow with convective heat transport in the presence of SWCNTs and MWCNTs is srutinized by Haq et al. [4]. The presence of SWCNTs and MWCNTs in this investigation plays an imperative role in the enhancement of thermal conductivity. Three-dimensional slip flow of SWCNT and MWCNT nanomaterials over a variable thicked surface is studied by Hayat et al. [5]. They have also utilized homogeneous and heterogeneous reactions to regulate the surface temperature. Further their theoretical outcomes presented that heat transfer rate is larger in case of MWCNT + water when compared with SWCNT + water. Recently some representative attempts for flows of SWCNTs and MWCNTs have been presented in Refs. [6–15] and numerous investigations therein.

Thermal motion of the charged particles produces electromagnetic radiation called thermal radiation. Every matter emits thermal radiation at a temperature greater than absolute zero (absolute temperature is also called thermodynamic temperature). When the absolute temperature is less than the body temperature, kinetic energy of molecules change due to inter-atomic collisions. Heat transfer in the presence of thermal radiation has many applications in physics, industrial engineering, space technology for example gas cooled nuclear reactors, aerodynamics rockets, large open water reservoirs, thermal power engineering and so forth. Rosseland approximation has been considered by numerous researchers for radiation effect. This type of approximation

* Corresponding author.
E-mail address: sirajsafi151@gmail.com (S. Ullah).

https://doi.org/10.1016/j.rinp.2017.12.017
2211-3797/

Nomenclature

u, v	Velocity components	T_m	Melting temperature
C_p	Specific heat	T_∞	Ambient temperature
U_w	Stretching velocity	K	Specific permeability
ν_{nf}	Kinematic viscosity of nanofluid	μ_{nf}	Nanofluid dynamic viscosity
σ^*	Stefan-Boltzman constant	ρ_{nf}	Nanofluid density
$(\rho c_p)_{nf}$	Heat capacity of nanoliquid	k_{nf}	Thermal conductivity of nanoliquid
q_w	Heat flux	l	Characteristics length
ϕ	Volume fraction of nanoparticles	U_e	Free stream velocity
β^*	Thermal expansion coefficient	μ_f	Dynamic viscosity
ρ_f	Nanofluid density	k^{dst}	Mean absorption coefficient
β_1	Slip parameter	γ	Curvature parameter
σ^*	Stefan-Boltzman constant	Pr	Prandtl number
Re_x	Reynold number	M	Melting parameter
Nr	Radiation parameter	ω	Porosity parameter
θ_w	Temperature ratio variable	κ	Specific or intrinsic permeability
Nu_x	Nusselt number	C_{fx}	Skin friction coefficient
τ_w	Shear stress	q_r	Radiative flux
k	Thermal conductivity		

comprises dimensionless variables called radiation parameter and Prandtl number which are supportable for linearized Rosseland approximation if the temperature difference between the plate and ambient liquid is small. However if the difference is larger than it is valid for non-linearized Rosseland approximation. Radiative flow over a stretched surface is examined by Cortell. [16]. Sheikholeslami et al. [17] investigated MHD two phase nanoliquid flow with thermal radiation. Reddy et al. [18] examined the impact of nonlinear radiation in three-dimensional MHD flow of ferromagnetic liquid subject to temperature dependent viscosity. Natural convection along a vertical isothermal plate with linear and nonlinear thermal radiations is studied by Pantokratoras [19]. Consequences of nonlinear thermal radiation and heterogeneous-homogeneous reactions in flow based on $Ag–H_2O$ and $Cu–H_2O$ nanomaterial by a stretched cylinder is presented by Qayyum et al. [20]. Nonlinear radiative flow with temperature dependent viscosity in thin liquid film towards a stretched surface is examined by Pal and Saha [21]. Significance of nonlinear radiation in mixed convection flow of magneto Walter-B nanoliquid is explored by Khan et al. [22]. Mixed convective flow with nonlinear thermal radiation of Oldroyd-B liquid near a stagnation region is studied by Hayat et al. [23]. MHD nanoliquid slip flow with entropy generation and nonlinear thermal radiation in a porous vertical microchannel is considered by López et al. [24]. Simultaneous effect of gyrotactic microorganisms and nonlinear thermal radiation on Magneto-Burgers nanomaterial is srutinized by Khan et al. [25].

Present work aims to model two-dimensional flow of SWCNTs and MWCNTs with Darcy-Forchheimer porous medium. Heat transfer process is explored subject to nonlinear thermal radiation, melting heat transport and viscous dissipation. Outcomes for SWCNT + Water and MWCNT + Water are achieved and compared. Xue model [15] is employed. The resulting nonlinear expressions are solved via Shooting method [26–36]. Velocity and temperature gradients are computed numerically and analyzed through in Tables 2 and 3.

Simulation of governing problems

Here two-dimensional steady and incompressible flow of water based carbon nanotubes is considered. Flow is due to nonlinear stretching surface. Xue model [15] is accomplished for nanomaterial transport mechanism. Nonlinear thermal radiation and dissipation effect are accounted. Flow in porous space is characterized by Darcy-Forchheimer relation. Here cylindrical coordinates are chosen in such manner that r-axis is along radial direction while x-axis is along axial direction (see Fig. 1). The governing expressions for mass and momentum are

$$\frac{\partial(rv)}{\partial r}+\frac{\partial(ru)}{\partial x}=0, \tag{1}$$

$$v\frac{\partial u}{\partial r}+u\frac{\partial u}{\partial x}=U_e\frac{dU_e}{dx}+\nu_{nf}\left(\frac{\partial^2 u}{\partial r^2}+\frac{1}{r}\frac{\partial u}{\partial r}\right)+\frac{\nu_{nf}}{\kappa}(U_e-u)+g\beta_T(T-T_m), \tag{2}$$

$$(\rho c_p)_{nf}\left(v\frac{\partial T}{\partial r}+u\frac{\partial T}{\partial x}\right)=k_{nf}\frac{1}{r}\frac{\partial}{\partial r}\left(r\frac{\partial T}{\partial r}\right)-\frac{\partial}{\partial r}(q_r)+\mu\left(\frac{\partial u}{\partial r}\right)^2, \tag{3}$$

With

$$\left.\begin{aligned} &u=U_w(x)+\delta_1\tfrac{\partial u}{\partial r},\ v=0,\ T=T_m,\ \text{at } r=R\\ &u\to U_e(x)=\tfrac{U_\infty x}{l},\ T\to T_\infty,\ \text{at } r\to\infty, \end{aligned}\right\} \tag{4}$$

$$k_{nf}\left(\frac{\partial T}{\partial r}\right)_{r=R}=\rho_{nf}[\lambda_1+c_s(T_m-T_0)]v(R,x). \tag{5}$$

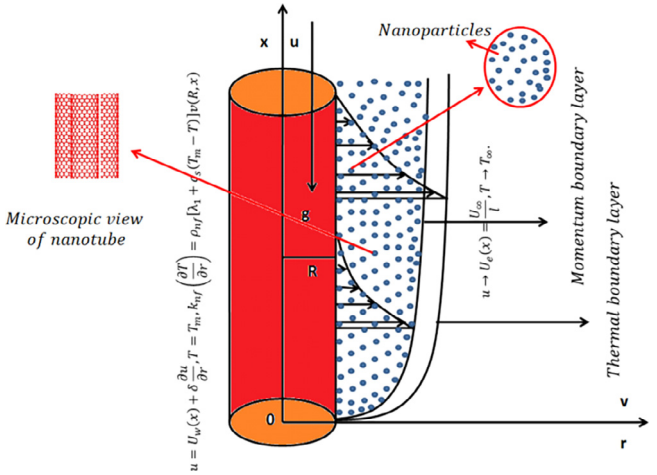

Fig. 1. Schematic flow diagram.

Here u, v represent velocity components, R radius, ρ density, U_e free stream velocity, κ permeability, U_w stretching velocity, ν_{nf} kinematic viscosity, k_{nf} thermal conductivity, c_p specific heat, β_T coefficient of thermal expansion, T temperature, q_r radiative heat flux, l characteristic length, δ_1 velocity slip, λ_1 latent heat and c_s heat capacity.

By Xue [15] one has

$$\left.\begin{gathered}\mu_{nf}=\frac{\mu_f}{(1-\phi)^{2.5}},\ \nu_{nf}=\frac{\mu_{nf}}{\rho_{nf}},\ \rho_{nf}=\rho_f(1-\phi)+\rho_s\phi,\\ (\rho c_p)_{nf}=(\rho c_p)_f(1-\phi)+(\rho c_p)_s\phi,\ \frac{k_{nf}}{k_f}=\frac{k_s+2k_f-2\phi(k_f-k_s)}{k_s+2k_f+2\phi(k_f-k_s)},\\ (\rho\beta)_{nf}=(\rho\beta)_f(1-\phi)+(\rho\beta)_s\phi,\end{gathered}\right\}\tag{6}$$

where μ_{nf} represents dynamic viscosity, ϕ volume fraction of nanoparticle, ρ_f and ρ_s densities of liquid and solid particles, k_f thermal conductivity of continuous phase liquid, k_{nf} thermal conductivity of nanoliquid, k_s thermal conductivity of carbon nanotubes, $(c_p)_{nf}$, $(c_p)_f$ and $(c_p)_s$ represent specific heat of nanofluid, base fluid and CNTs respectively.

The radiative heat flux in terms of Rosseland approximation is [20]:

$$q_r=-\frac{4\sigma^*}{3k^*}\frac{\partial T^4}{\partial r}=-\frac{16\sigma^*}{3k^*}T^3\frac{\partial T}{\partial r},\tag{7}$$

In above expression k^* denotes the mean absorption coefficient and σ^* denotes the Stefan-Boltzman constant.

Considering

$$\left.\begin{gathered}\eta=\frac{r^2-R^2}{2R}\sqrt{\frac{U_0}{\nu_f l}},\ u=\frac{xU_0}{l}f'(\eta),\ v=\frac{-R}{r}\sqrt{\frac{\nu_f U_0}{l}}f(\eta),\\ \theta=\frac{T-Tm}{T_\infty-T_m},\ \psi(\eta)=\sqrt{U_w\nu_f xR}f(\eta),\end{gathered}\right\}\tag{8}$$

Eq. (1) is automatically verified and Eqs. (2)–(4) yield

$$\left.\begin{gathered}\frac{1}{(1-\phi)^{2.5}\left(1-\phi+\frac{\rho_c}{\rho_f}\phi\right)}((1+2\gamma\eta)f'''+2\gamma f'')+\frac{\omega}{(1-\phi)^{2.5}\left(1-\phi+\frac{\rho_c}{\rho_f}\phi\right)}(A-f')\\ +\lambda\left(\frac{1-\phi+\frac{(\rho\beta)c}{(\rho\beta)_f}\phi}{1-\phi+\frac{\rho_c}{\rho_f}\phi}\right)\theta-f'^2+ff''+A^2=0,\end{gathered}\right\}\tag{9}$$

$$\left.\begin{gathered}\frac{k_{nf}}{k_f}\frac{1}{\Pr\left(1-\phi+\frac{(\rho c_p)_c}{(\rho c_p)_f}\phi\right)}(2\gamma\theta'+(1+2\gamma\eta)\theta'')\\ +Nr\frac{1}{\Pr\left(1-\phi+\frac{(\rho c_p)_c}{(\rho c_p)_f}\phi\right)}(\theta(\theta_w-1)+1)^2\{(3\theta'^2(1+2\gamma\eta)(\theta_w-1)\\ +2\gamma\theta'(\theta(\theta_w-1)+1)+\theta''(1+2\gamma\eta)(\theta(\theta_w-1)+1))\}\\ +\frac{Ec}{(1-\phi)^{2.5}}\left(1-\phi+\frac{(\rho c_p)_c}{(\rho c_p)_f}\phi\right)(1+2\gamma\eta)f'''+f\theta'=0,\end{gathered}\right\}\tag{10}$$

$$\left.\begin{gathered}f'(0)=1+\frac{\beta^*}{(1-\phi)^{2.5}}f''(0),\ \theta(0)=0,\ f'(\infty)=A,\ \theta(\infty)=1,\\ \Pr\left(1-\phi+\frac{\rho_c}{\rho_f}\phi\right)f(0)+M\frac{k_{nf}}{k_f}\theta'(0)=0.\end{gathered}\right\}\tag{11}$$

In above expressions $\gamma\left(=\sqrt{\frac{l\nu_f}{U_0R^2}}\right)$ represents the curvature parameter, $\Pr\left(=\frac{(\rho c_p)_f\nu_f}{k_f}\right)$ the Prandtl number, $\omega\left(=\frac{l\nu_f}{U_0K}\right)$ the porosity parameter, $\lambda\left(=\frac{Gr}{Re^2x}\right)$ the mixed convection parameter,

Table 1
Physical properties for nanomaterials and continuous phase liquid.

Thermophysical characteristics	Base fluid	Nanomaterials	
	Water	SWCNT	MWCNT
$\rho(kg/m^3)$	997	2600	1600
$c_p(j/kgK)$	4179	425	796
$k(w/mK)$	0.613	6600	3000

Table 2
Numerical results of $\left(Cf_x\,\mathrm{Re}_x^{\frac{1}{2}}\right)$ for different physical variables.

β	γ	φ	M	Nr	E_c	ω	λ	$-Cf_x\mathrm{Re}_x^{\frac{1}{2}}$	
								SWCNT	MWCNT
0.2	0.1	0.2	0.5	0.8	0.2	0.3	0.4	2.10241	2.00891
0.3								1.83279 ↑	1.76078
0.5								1.46558	1.41816
	0.2							2.16560	2.07755
	0.3							2.22733 ↓	2.14422
	0.5							2.34738	2.27301
		0.1						1.69711	1.64382
		0.2						2.10241 ↓	2.00891
		0.4						3.19893	3.06856
			0.1					2.16861	2.06994
			0.3					2.13343 ↑	2.03721
			0.6					2.08819	1.99610
				0.1				2.10069	2.00583
				0.3				2.10137 ↓	2.00697
				0.8				2.10241	2.00891
					0.1			2.10785	2.01424
					0.4			2.09163 ↑	1.99835
					0.8			2.07048	1.97763
						0.1		1.90253	1.79033
						0.2		2.00575 ↓	1.90354
						0.3		2.10241	2.00891
							0.1	2.24562	2.16071
							0.2	2.19748 ↑	2.1098
							0.4	2.10241	2.00891

Table 3
Numerical results of $\left(Nu_x\,\mathrm{Re}_x^{-\frac{1}{2}}\right)$ for different physical variables.

β	γ	φ	M	Nr	E_c	ω	λ	$\mathrm{Nu}_x\mathrm{Re}_x^{-\frac{1}{2}}$	
								SWCNT	*MWCNT*
0.1	0.1	0.2	0.5	0.8	0.2	0.3	0.4	−3.80678	−3.62052
0.2								−3.61127 ↓	−3.43972 ↓
0.4								−3.37152	−3.21237
	0.2							−3.97809	−3.95358
	0.3							−4.3378 ↑	−4.09406 ↑
	0.5							−5.0327	−4.72631
		0.1						−2.92526	−3.16401
		0.2						−3.61127 ↑	−3.43972 ↑
		0.4						−5.73744	−5.28077
			0.2					−3.93643	−4.36895
			0.3					−3.82012 ↓	−3.67172 ↓
			0.6					−3.51703	−3.33663
				0.1				−3.14981	−3.38921
				0.4				−3.34662 ↑	−3.17481 ↑
				0.8				−3.61127	−3.43972
					0.1			−3.47514	−3.77364
					0.4			−3.88065 ↑	−3.68915 ↑
					0.8			−4.40807	−4.17676
						0.1		−3.66602	−3.98068
						0.2		−3.63735 ↓	−3.96615 ↓
						0.4		−3.58744	−3.94266
							0.1	−3.56499	−3.94302
							0.2	−3.57975 ↑	−3.94559 ↑
							0.4	−3.61127	−3.95358

$Gr\left(=\frac{g\beta(T_m-T_\infty)x^3}{\nu_f^2}\right)$ the Grashof number, $Nr\left(=\frac{16\sigma^* T_\infty^3}{3k^* k_f}\right)$ the radiation parameter, $\theta_w\left(=\frac{T_\infty}{T_m}\right)$ the temperature ratio parameter, $Ec\left(=\frac{U_w^2}{(c_p)_f(T_\infty-T_m)}\right)$ the Eckert number and $\beta^*\left(=\delta\left(U_0\rho_f l\right)^{\frac{1}{2}}\right)$ the slip parameter.

Mathematical form for velocity and temperature gradients are

$$\left.\begin{aligned} C_{fx} &= \frac{2\tau_w}{\rho_f U_w^2},\\ Nu_x &= \frac{xq_w}{k_f(T_w-T_\infty)}, \end{aligned}\right\} \tag{12}$$

where τ_w the shear stress and q_w the surface heat flux and defined as

$$\left.\begin{aligned} \tau_w &= \mu_{nf}\left(\frac{\partial u}{\partial r}\right)\Big|_{r=R},\\ q_w &= -k_{nf}\left(\frac{\partial T}{\partial r}\right)\Big|_{r=R} + (q_r)_w. \end{aligned}\right\} \tag{13}$$

Invoking Eq. (13) into Eq. (12) we get

$$C_f\mathrm{Re}_x^{0.5} = \frac{2f''(0)}{(1-\phi)^{2.5}}, \tag{14}$$

$$Nu_x\mathrm{Re}_x^{-0.5} = -\left(\frac{k_{nf}}{k_f} + Nr(\theta(0)(\theta_w-1)+1)^3\right)\theta'(0), \tag{15}$$

where $\mathrm{Re}_x = \frac{U_w x}{\nu_f}$ represents the local Reynold number.

Computational treatment

To solve Eqs. (9) and (10) with boundary conditions (11) numerically, we have apply Built-in-shooting method. This method is well tested procedure to find out the results of ODEs.

Discussion

The objectives of this portion is to investigate the impacts of different physical variables like curvature parameter (γ), porosity parameter (ω), mixed convection parameter (λ), ratio parameter (A), radiation parameter (Nr), melting parameter (M), volume fraction (ϕ), temperature ratio variable (θ_w) and Eckert number (Ec) on the velocity $(f'(\eta))$ and temperature $(\theta(\eta))$ for both SWCNTs and MWCNTs. Table 1 represents the thermophysical characteristics of continuous phase fluid and SWCNTs and MWCNTs. Table 2 presents the numerical data for surface drag force $\left(C_{fx}\mathrm{Re}_x^{0.5}\right)$ for larger values of (Ec), (ω), (λ), (Nr), (γ), (ϕ) and (M) subject to SWCNTs and MWCNTs. Here $\left(C_{fx}\mathrm{Re}_x^{0.5}\right)$ is higher for larger estimation of M, γ, φ, Nr *and* ω. While the reverse trend is observed for Ec, λ and β for both SWCNTs and MWCNTs. Table 3 provides the computational results for heat transfer rate $\left(Nu_x\mathrm{Re}^{-\frac{1}{2}}\right)$ for varying (Ec), (ω), (λ), (Nr), (γ), (ϕ) and (M) in both SWCNTs and MWCNTs cases. It is examined that rate of heat transfer enhances for different estimations of (Ec), (M), (β), *and* λ while it decays for (γ), ω, Nr,

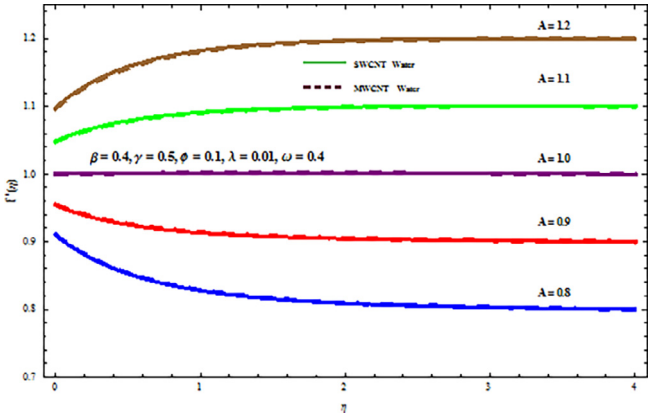

Fig. 2. $f'(\eta)$ via A.

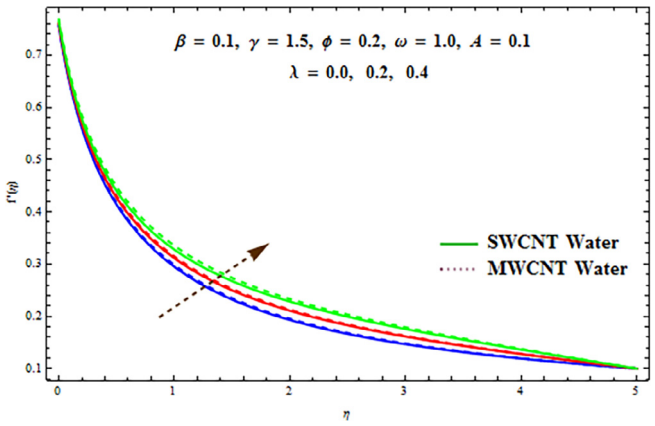

Fig. 3. γ via λ.

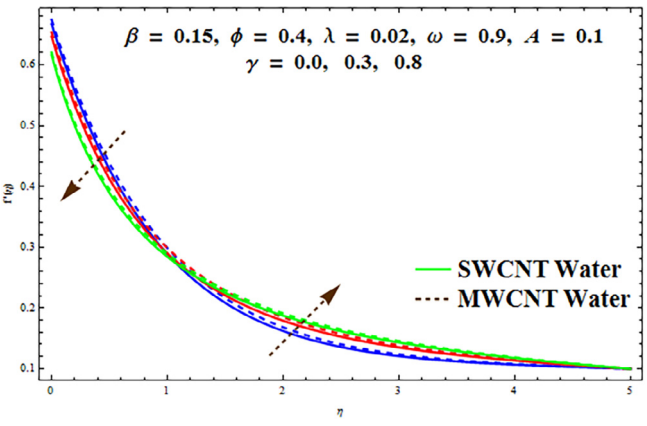

Fig. 6. $f'(\eta)$ via γ.

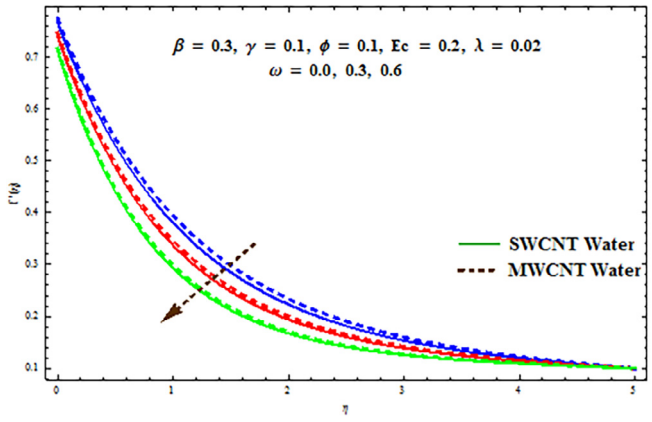

Fig. 4. $f'(\eta)$ via ω.

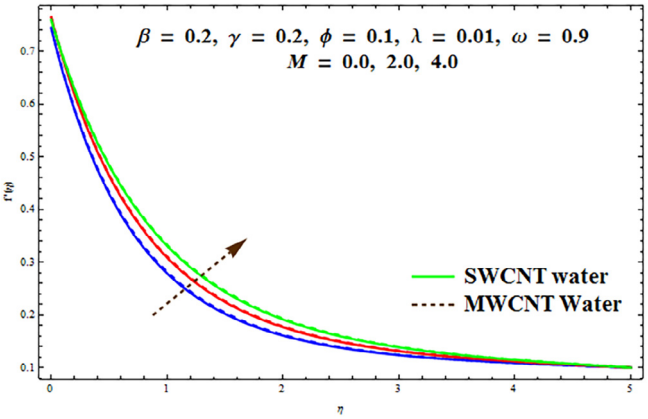

Fig. 7. $f'(\eta)$ via M.

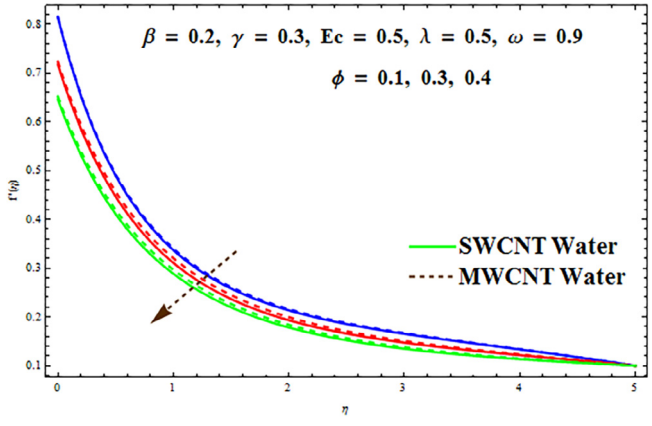

Fig. 5. $f'(\eta)$ via ϕ.

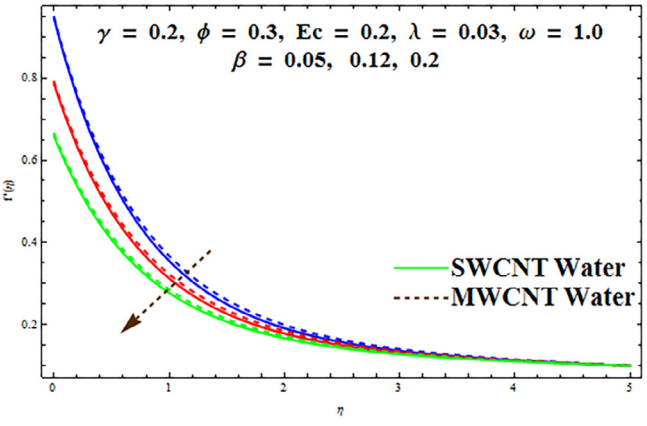

Fig. 8. $f'(\eta)$ via β.

Ec and ω. Behavior of (A) on $(f'(\eta))$ is pictured in Fig. 2. Here $(f'(\eta))$ enhances for both SWCNTs and MWCNTs. Here no boundary layer exists for $A = 1$. In fact both fluid and cylinder move at the same velocity. It is also pointed out that $(f'(\eta))$ have distinct values on the surface of cylinder due to slip condition. Characteristics of (λ) on $(f'(\eta))$ is shown in Fig. 3. Here velocity $f'(\eta)$ and layer thickness are enhanced for higher (λ). physically (λ) is the ratio of inertial to buoyancy forces. Therefore for various values of (λ) buoyancy force enhances and as a result $(f'(\eta))$ boosts. Fig. 4 demonstrates effect of porosity variable (ω) on $(f'(\eta))$. Here reduction in $(f'(\eta))$ is noticed for higher (ω), Variation in velocity $(f'(\eta))$ for higher (ϕ) is shown in Fig. 5. It can be noticed that $(f'(\eta))$ decays with (ϕ) for both SWCNTs and MWCNTs. It is also marked that $(f'(\eta))$ of nanoliquid is larger than of pure liquid $(\phi = 1)$. Effect of (γ) on $(f'(\eta))$ is displayed in Fig. 6. Here both velocity and momentum layer thickness decrease near surface of cylinder while contrast effects are observed away from the surface of cylinder. Also radius of cylinder

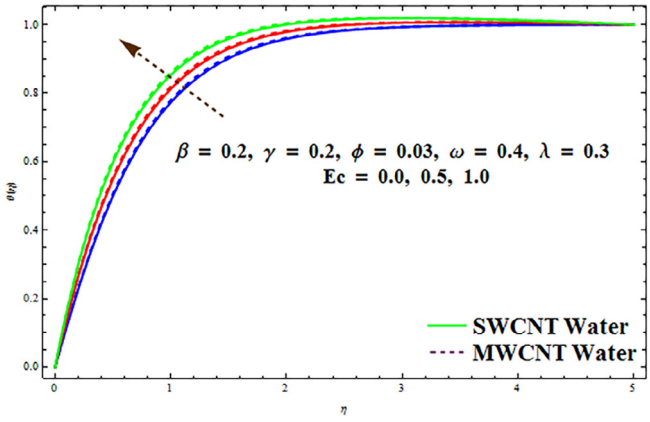

Fig. 9. $\theta(\eta)$ via *Ec*.

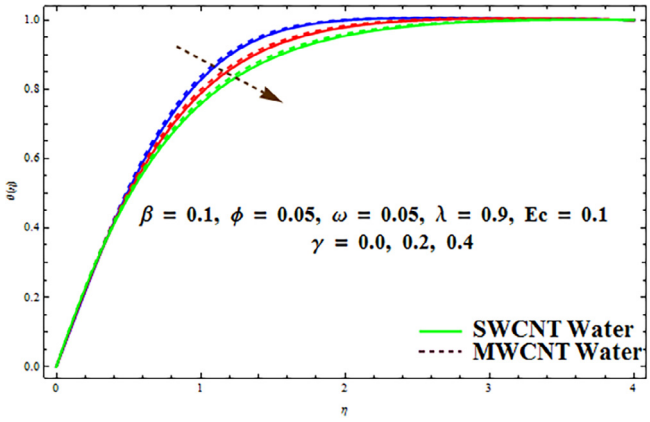

Fig. 10. $\theta(\eta)$ via γ.

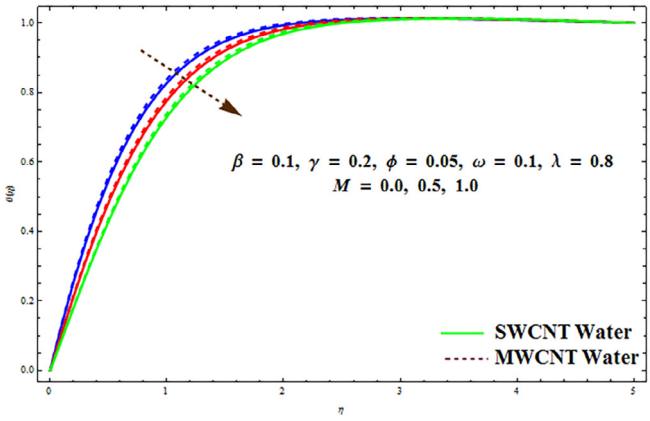

Fig. 11. $\theta(\eta)$ via M.

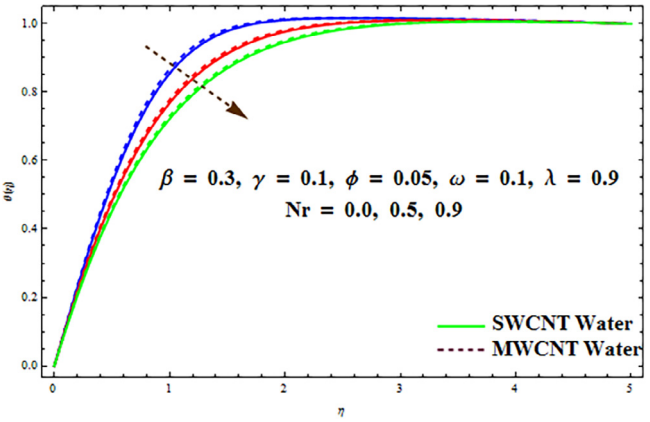

Fig. 12. $\theta(\eta)$ via *Nr*.

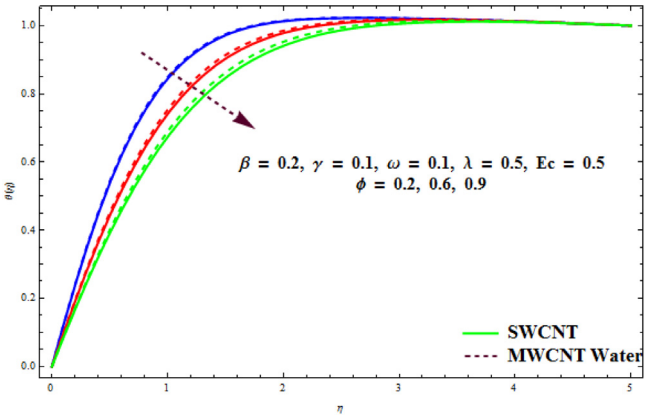

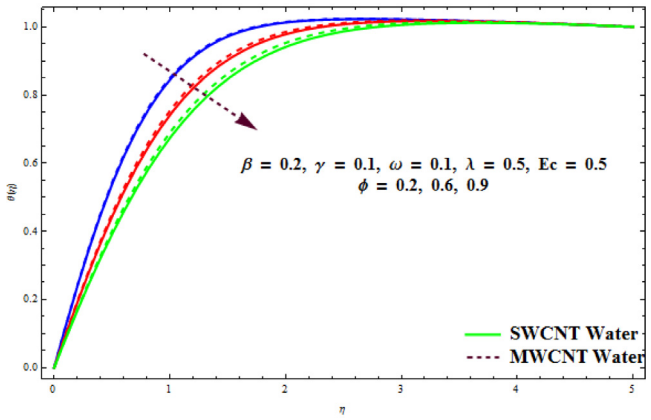

Fig. 13. $\theta(\eta)$ via ϕ.

R decreases for larger curvature parameter(γ). Therefore less particles accommodate on the cylinder surface and as a results less resistance provides to fluid particle. That is why $(f'(\eta))$ increases away from the surface of cylinder. Fig. 7 Indicates that the larger estimations of (M) causes an increase in $(f'(\eta))$ for both SWCNTs and MWCNTs. In fact larger values of (M) lead more heat transport from heated liquid to cold melting surface of cylinder due to the high convection. Therefore velocity and momentum layer thickness increase. Influence of slip parameter (β) on $(f'(\eta))$ is sketched in Fig. 8. Here both velocity and associated layer thickness decay for higher (β). Moreover $(f'(\eta))$ dominants in case of MWCNTs when compared with SWCNTs. Fig. 9 Captures the influence of Eckert number (Ec) on $(\theta(\eta))$. Temperature is increasing function of higher estimation of Eckert number (Ec). Also thermal layer thickness increases for both SWCNTs and MWCNTs. $\theta(\eta)$ against curvature variable (γ) is exhibited in Fig. 10. Here $(\theta(\eta))$ show dual behavior for larger (γ). with an enhancement in curvature parameter radius of cylinder decays and as a result temperature increases near the surface of cylinder. Temperature diminishes as the radius of cylinder enhances. Consequences of melting parameter (M) on $\theta(\eta)$ is depicted in Fig. 11. Here temperature increases for both SWCNTs and MWCNTs for higher values of (M). It is also investigated that thermal layer thickness enhances for higher melting

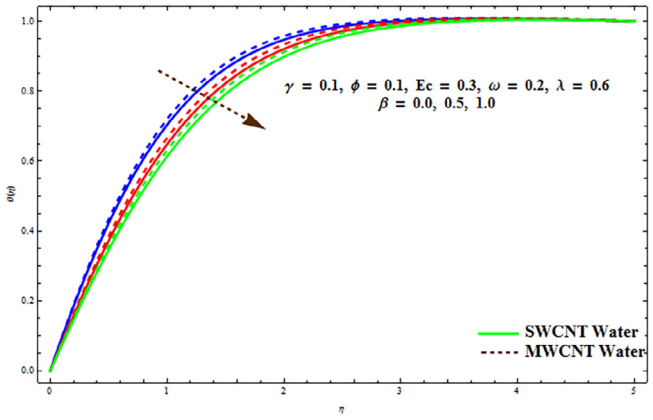

Fig. 14. $\theta(\eta)$ via β.

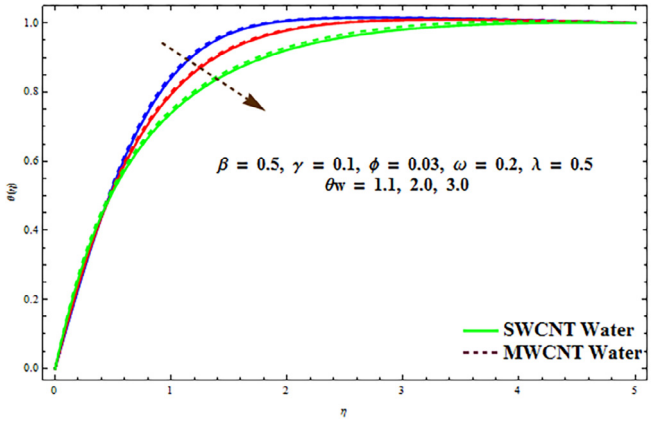

Fig. 15. $\theta(\eta)$ via θ_w.

variable. Physically larger melting parameter (M) provides more heat from heated fluid surface to cold surface of cylinder. Fig. 12 depicts the change in temperature field $(\theta(\eta))$ for varying radiation parameter. An increase in (Nr) leads to higher temperature field for both cases *i.e.*, MWCNTs and MWCNTs. Generally larger values of (Nr) produce extra heat to operating liquid that shows associate improvements within$(\theta(\eta))$. Fig. 13 presents that rising values of nanoparticle volume fraction (ϕ) correspond to lower $(\theta(\eta))$ for both MWCNTs and MWCNTs. Physically higher estimations of (ϕ) result in an enhancement of heat transfer by convection phenomenon from heated fluid towards cold surface due to which temperature diminished. Influence of slip parameter (β) on $\theta(\eta)$ is shown in Fig. 14. It is observed that temperature along with thermal layer thickness reduce as (β) rises gradually. Since with the increment in (β) the rate of heat transfer at the surface increases. Therefore temperature field declines. Fig. 15 illustrates effect of (θ_w) on $\theta(\eta)$. Clearly temperature field is a decreasing function of (θ_w) .

Conclusions

The main conclusions drawn from the study are as follows:

- Velocity field decreases via (ϕ) and (ω).
- Larger estimation of (M) and (λ) leads to increase of $f'(\eta)$ and momentum layer thickness.
- Both $f'(\eta)$ and $\theta(\eta)$ show dual nature for rising values of (γ).
- Temperature field decays for larger (M), (β) and (Nr). Higher estimations of (M) and (Nr) increase the rate of heat transfer as well as thermal layer. $(Cf_x\mathrm{Re}_x^{\frac{1}{2}})$ decreases for large a (ϕ) and it enhances via (M) and (Ec).

Acknowledgments

We are grateful to Higher Education Commission (HEC) of Pakistan for financial Support of this work under the project No. 20-3038/NRPU/R & D/HEC/13.

References

[1] Choi SUS, Zhang ZG, Yu W, Lockwood FE, Grulke EA. Anomalous thermal conductivity enhancement in nanotube suspensions. AIP Appl Phys Lett 2001;79:2252.
[2] Hayat T, Kiran A, Imtiaz M, Alsaedi A. Unsteady flow of carbon nanotubes with chemical reaction and Cattaneo-Christov heat flux model. Results Phys 2017;7:823–31.
[3] Mahanthesh B, Gireesha BJ, Shashikumar NS, Shehzad SA. Marangoni convective MHD flow of SWCNT and MWCNT nanoliquids due to a disk with solar radiation and irregular heat source. Phys E Low-dimensional Syst Nanostruct 2017;94:25–30.
[4] Haq RU, Nadeem S, Khan ZH, Noor NFM. Convective heat transfer in MHD slip flow over a stretching surface in the presence of carbon nanotubes. Phys B Condens Matter 2015;457:40–7.
[5] Hayat T, Hussain Z, Alsaedi A, Ahmad B. Numerical study for slip flow of carbon-water nanofluids. Comput Methods Appl Mech Eng 2017;319:366–78.
[6] Hayat T, Khan MI, Waqas M, Alsaedi A, Farooq M. Numerical simulation for melting heat transfer and radiation effects in stagnation point flow of carbon–water nanofluid. Comput Methods Appl Mech Eng 2017;315:1011–24.
[7] Dharmalingam R, Kandasamy R, Prabhu KKS. Lorentz forces and nanoparticle shape on water based Cu, Al2O3 and SWCNTs. J Mol Liq 2017;231:663–72.
[8] Hayat T, Naseem A, Khan MI, Farooq M, Saedi A. Magnetohydrodynamic (MHD) flow of nanofluid with double stratification and slip conditions. Phys Chem Liq 2017. https://doi.org/10.1080/00319104.2017.1317778.
[9] Hayat T, Qayyum S, Imtiaz M, Alzahrani F, Alsaedi A. Partial slip effect in flow of magnetite-Fe3O4 nanoparticles between rotating stretchable disks. J Magn Magn Mater 2016;413:39–48.
[10] Arabghahestani M, Karimian SMH. Molecular dynamics simulation of rotating carbon nanotube in uniform liquid argon flow. J Mol Liq 2017;225:357–64.
[11] Hayat T, Khan MI, Farooq M, Alsaedi A, Yasmeen T. Impact of Marangoni convection in the flow of carbon-water nanofluid with thermal radiation. Int J Heat Mass Transf 2017;106:810–5.
[12] Hayat T, Muhammad K, Farooq M, Alsaedi A. Melting heat transfer in stagnation point flow of carbon nanotubes towards variable thickness surface. AIP Adv 2016;6:015214.
[13] Hayat T, Muhammad K, Farooq M, Alsaedi A. Unsteady Squeezing Flow of Carbon Nanotubes with Convective Boundary Conditions. Plos One 2016;11:0152923.
[14] Hayat T, Khan MI, Farooq M, Yasmeen T, Alsaedi A. Water-carbon nanofluid flow with variable heat flux by a thin needle. J Mol Liq 2016;224:786–91.
[15] Haq RU, Shahzad F, Mdallal QMA. MHD pulsatile flow of engine oil based carbon nanotubes between two concentric cylinders. Results Phys 2017;7:57–68.
[16] Xue QZ. Model for thermal conductivity of carbon nanotube-based composites. Phys B Condens Matter 2005;368:302–7.
[17] Cortell R. Fluid flow and radiative nonlinear heat transfer over a stretching sheet. J King Saud Univ Sci 2014;26:161–7.
[18] Sheikholeslami M, Ganji DD, Javed MY, Ellahi R. Effect of thermal radiation on magnetohydrodynamics nanofluid flow and heat transfer by means of two phase model. J Magn Magn Mater 2015;374:36–43.
[19] Reddy JVR, Surunamma V, Sandeep N. Impact of nonlinear radiation on 3D magnetohydrodynamic flow of methanol and kerosene based ferrofluids with temperature dependent viscosity. J Mol Liquids 2017;236:39–100.
[20] Pantokratoras A. Natural convection along a vertical isothermal plate with linear and nonlinear Rosseland thermal radiation. Int J Therm Sci 2014;84:151–7.
[21] Qayyum S, Khan MI, Hayat T, Alsaedi A. A framework for nonlinear thermal radiation and homogeneous-heterogeneous reactions flow based on silver-water and copper-water nanoparticles: A numerical model for probable error. Results Phys 2017;7:1907–14.
[22] Pal D, Saha P. Influence of nonlinear thermal radiation and variable viscosity on hydromagnetic heat and mass transfer in a thin liquid film over an unsteady stretching surface. Int J Mech Sci 2016;119:208–16.
[23] Khan MI, Waqas M, Hayat T, Alsaedi A, Khan MI. Significance of nonlinear radiation in mixed convection flow of magneto Walter-B nanoliquid. Int J Hydrogen Energy 2017. In press.
[24] Hayat T, Qayyum S, Alsaedi A, Waqas M. Simultaneous influences of mixed convection and nonlinear thermal radiation in stagnation point flow of Oldroyd-B fluid towards an unsteady convectively heated stretched surface. J Mol Liq 2016;224:811–7.
[25] López A, Ibáñez G, Pantoja J, Moreira J, Lastres O. Entropy generation analysis of MHD nanofluid flow in a porous vertical microchannel with nonlinear thermal radiation, slip flow and convective-radiative boundary conditions. Int J Heat Mass Transf 2017;107:982–94.
[26] Khan M, Irfan M, Khan WA. Impact of nonlinear thermal radiation and gyrotactic microorganisms on the Magneto-Burgers nanofluid. Int J Mech Sci 2017;130:375–82.

[27] Hayat T, Khan MI, Shehzad SA, Khan MI, Alsaedi A. Numerical simulation of Darcy-Forchheimer flow of third grade liquid with Cattaneo-Christov heat flux model. Math Methods Appl Sci 2017. https://doi.org/10.1002/mma.4403.
[28] Khan MI, Waqas M, Hayat T, Alsaedi A. A comparative study of Casson fluid with homogeneous-heterogeneous reactions. J Colloid Interface Sci 2017;498:85–90.
[29] Hayat T, Tamoor M, Khan MI, Alsaedi A. Numerical simulation for nonlinear radiative flow by convective cylinder. Results Phys 2016;6:1031–5.
[30] Makinde OD, Khan WA, Khan ZH. Buoyancy effects on MHD stagnation point flow and heat transfer of a nanofluid past a convectively heated stretching/shrinking sheet. Int J Heat Mass Transf 2013;62:526–33.
[31] Khan MI, Kiyani MZ, Malik MY, Yasmeen T, Khan MWA, Abbas T. Numerical investigation of magnetohydrodynamic stagnation point flow with variable properties. Alexandria Eng J 2016;55:2367–73.
[32] Yasmeen T, Hayat T, Khan MI, Imtiaz M, Alsaedi A. Ferrofluid flow by a stretched surface in the presence of magnetic dipole and homogeneous-heterogeneous reactions. J Mol Liquids 2006;223:1000–5.
[33] Khan MI, Waqas M, Hayat T, Alsaedi A. Magneto-hydrodynamical numerical simulation of heat transfer in MHD stagnation point flow of Cross fluid model towards a stretched surfaces, Phys Chem Liquids, doi: 10.1080/00319104.2017.1367791.
[34] Khan MI, Waqas M, Hayat T, Khan MI, Alsaedi A. Numerical simulation of nonlinear thermal radiation and homogeneous-heterogeneous reactions in convective flow by a variable thicked surface. J Mol Liq 2017;246:259–67.
[35] Khan MI, Hayat T, Alsaedi A. Numerical analysis for Darcy-Forchheimer flow in presence of homogeneous-heterogeneous reactions. Results Phys 2017;7:2644–50.
[36] Hayat T, Khan MI, Farooq M, Alsaedi A, Waqas M, Yasmeen T. Impact of Cattaneo-Christov heat flux model in flow of variable thermal conductivity fluid over a variable thicked surface. Int J Heat Mass Transf 2016;99:702–10.